# Supplementary Materials: Zircon Chemistry and Oxidation State of Magmas for the Duobaoshan-Tongshan Ore-Bearing Intrusions in the Northeastern Central Asian Orogenic Belt, NE China

**Jian Wang *, Keiko Hattori, Yanchen Yang and Haiqi Yuan**

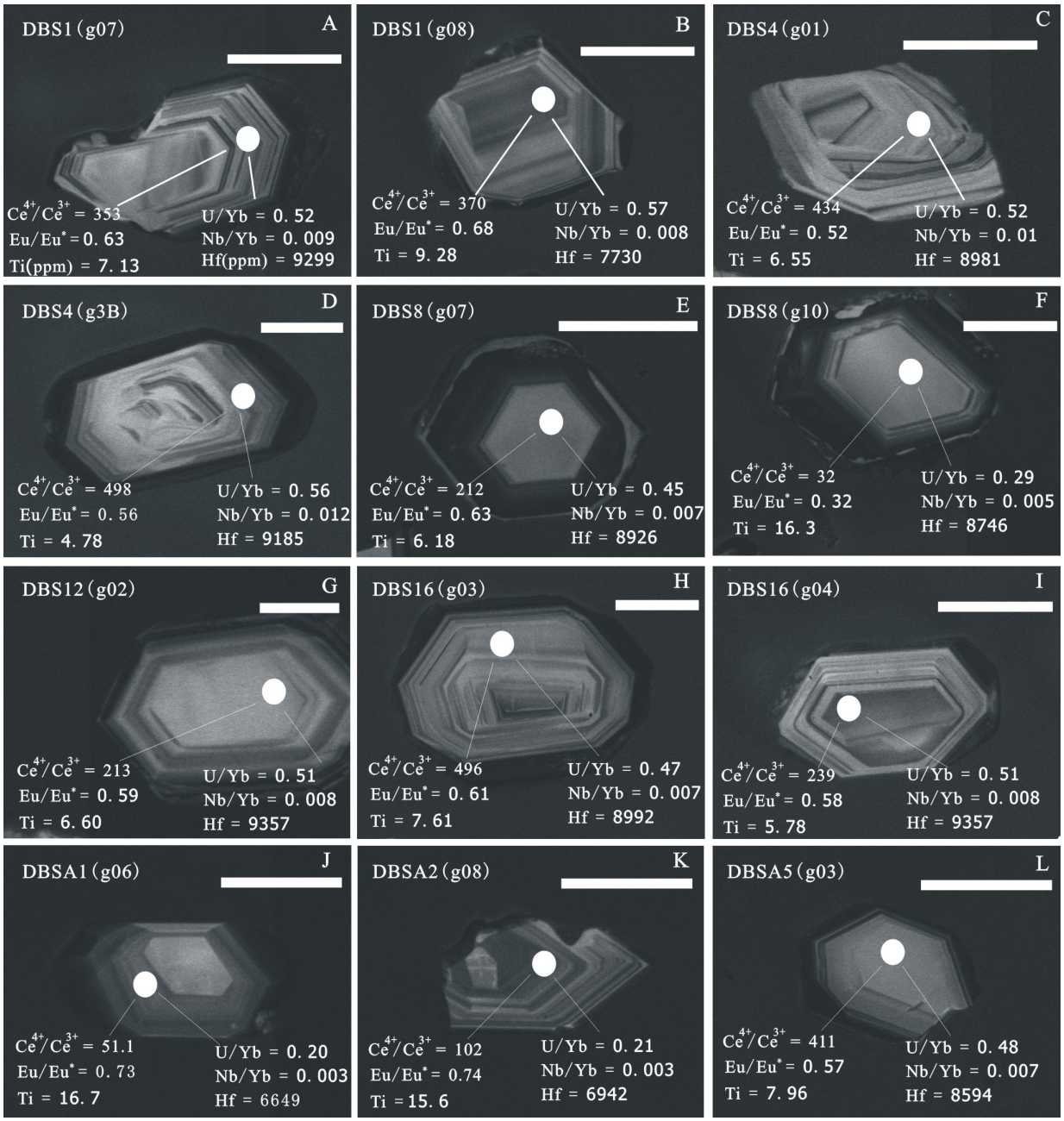


**Figure S1.** SEM-cathodoluminescence images of zircon grains from the DBS-TS ore-bearing microgabbroic, dioritic to granodioritic intrusions. CL images of zircon grains from the Mesozoic Qz-monzonite intrusion are also shown. Note: (**A–F**) are variably altered samples; (**G–I**, **L**) are mineralized samples; (**J, K**) are Mesozoic Qz-monzonites. Scale bar in all figures is 100 μm.

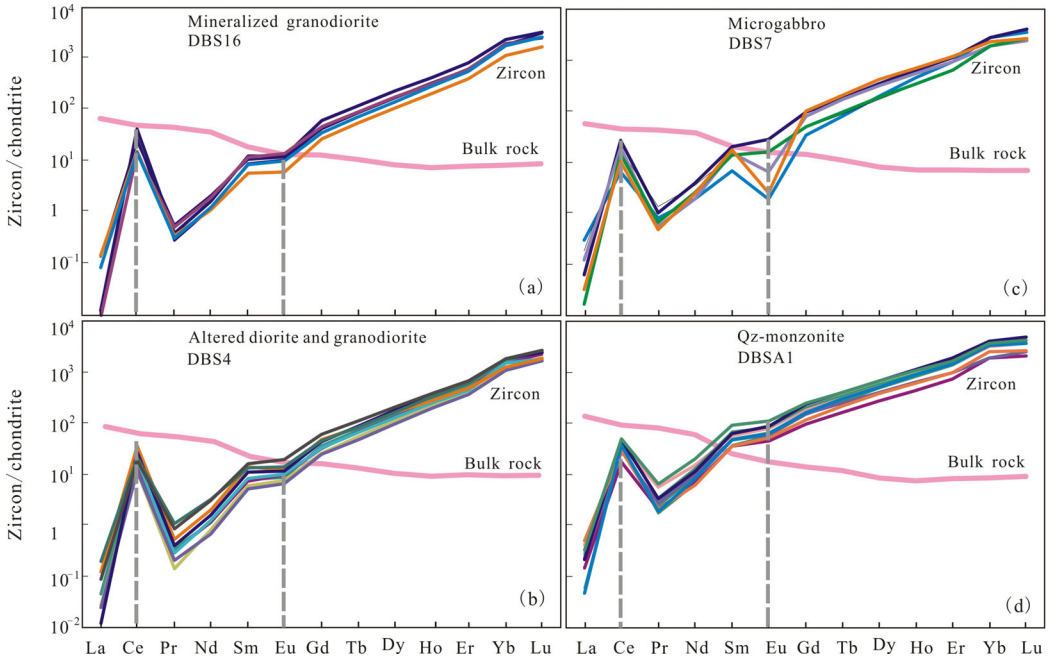


**Figure S2.** Chondrite-normalized REE patterns of zircon for a (**a**) representative sample (DBS16) of mineralized granodiorites, (**b**) representative sample (DBS4) of altered granodiorites, (**c**) representative sample (DBS7) of microgabbros, and (**d**) representative sample (DBSA1) of Qz-monzonites. Note the bulk rock REE patterns (bold pink lines) are also shown for comparison in the particular figure (Figure S2a–d).

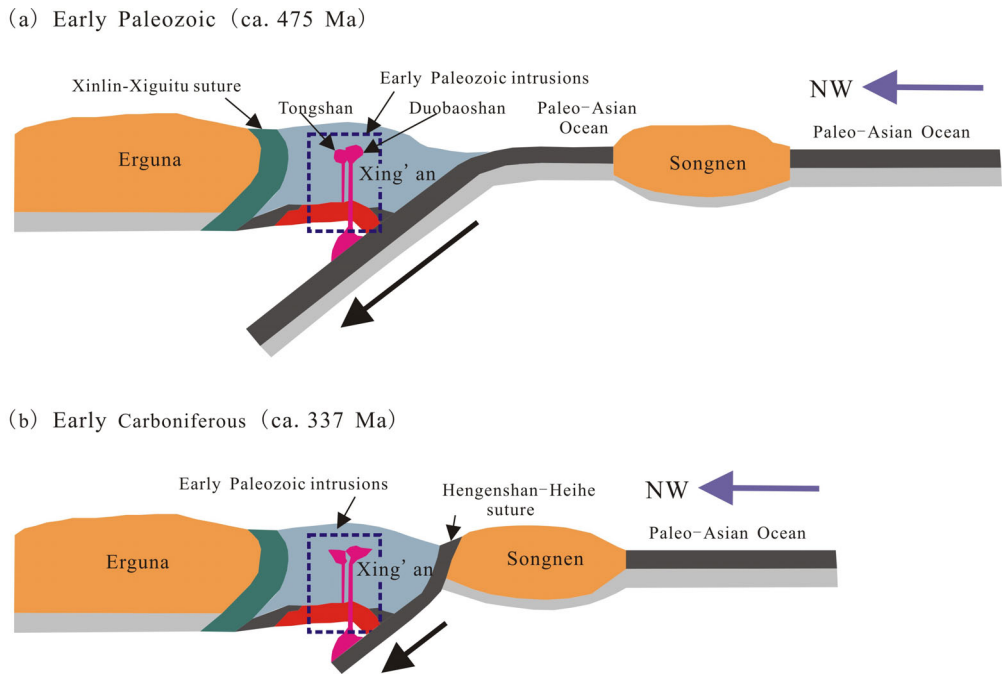


**Figure S3.** Evolution model for the Paleo-Asian Ocean and magmatism in NE China from (**a**) early Paleozoic to (**b**) early Carboniferous of the eastern CAOB (modified after [1,2]).

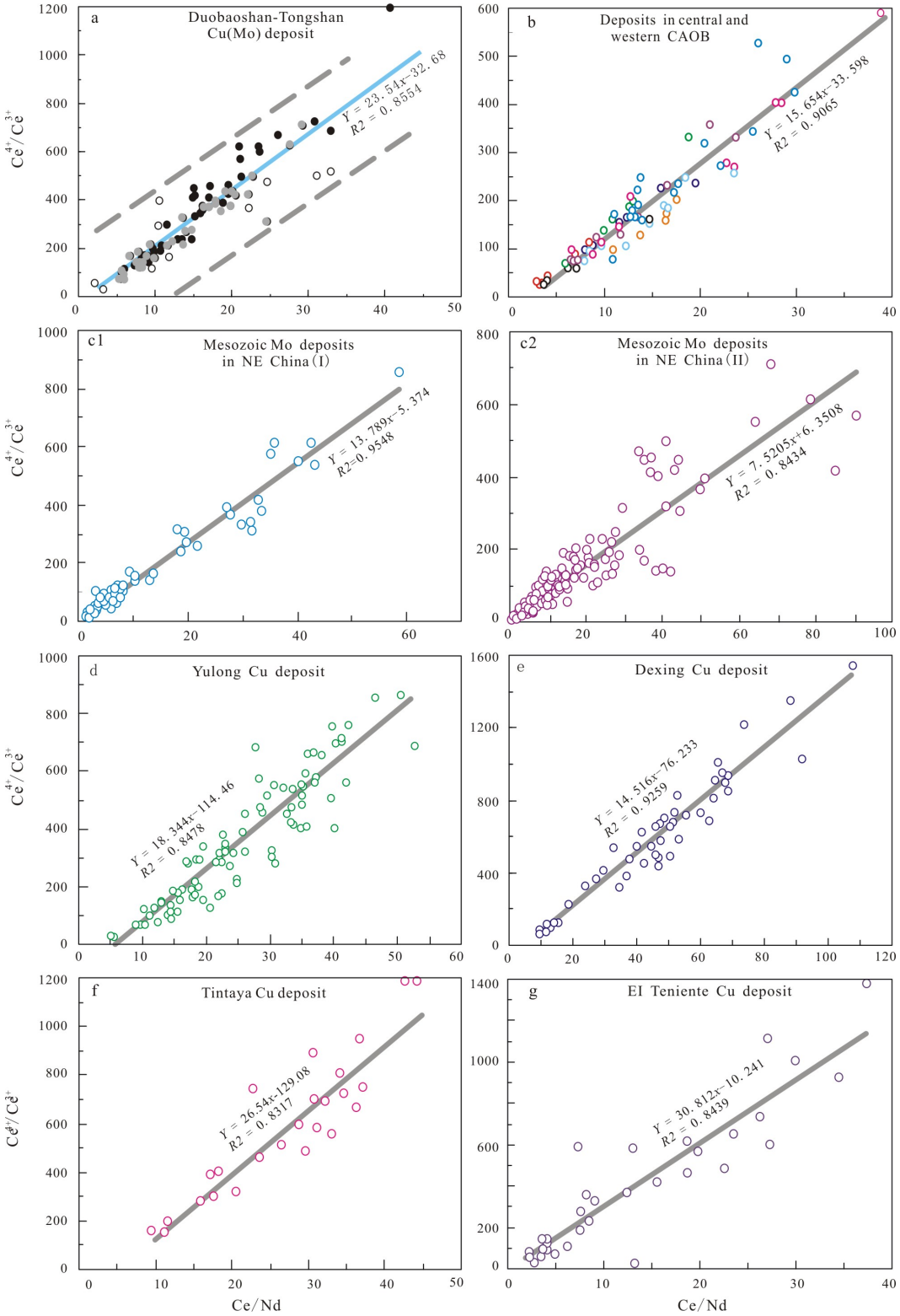


**Figure S4.** (**a**) Plot of $Ce^{4+}/Ce^{3+}$ versus Ce/Nd for zircons in the gabbroic, dioritic and granodioritic intrusions of the DBS-TS porphyry Cu-Mo deposit. Also shown for comparison include (**b**) deposits in central and western CAOB [3], (**c1, c2**) Mesozoic Mo deposits in NE China [4], (**d**) Yulong Cu deposit belt in eastern Tibet [5,6], (**e**) Dexing Cu deposit in SE China [7], (**f**) Tintaya Cu deposit in Peru [8,9], and (**g**) EI Teniente Cu deposit in Chile [10,11]. Note: 1) the colored symbols in each sufigure represent the compositions of zircon, with each circle representing one analysis of zircon grain. 2) symbols with different colors in Figure S4b represent zircon analyses from different deposits of the CAOB.

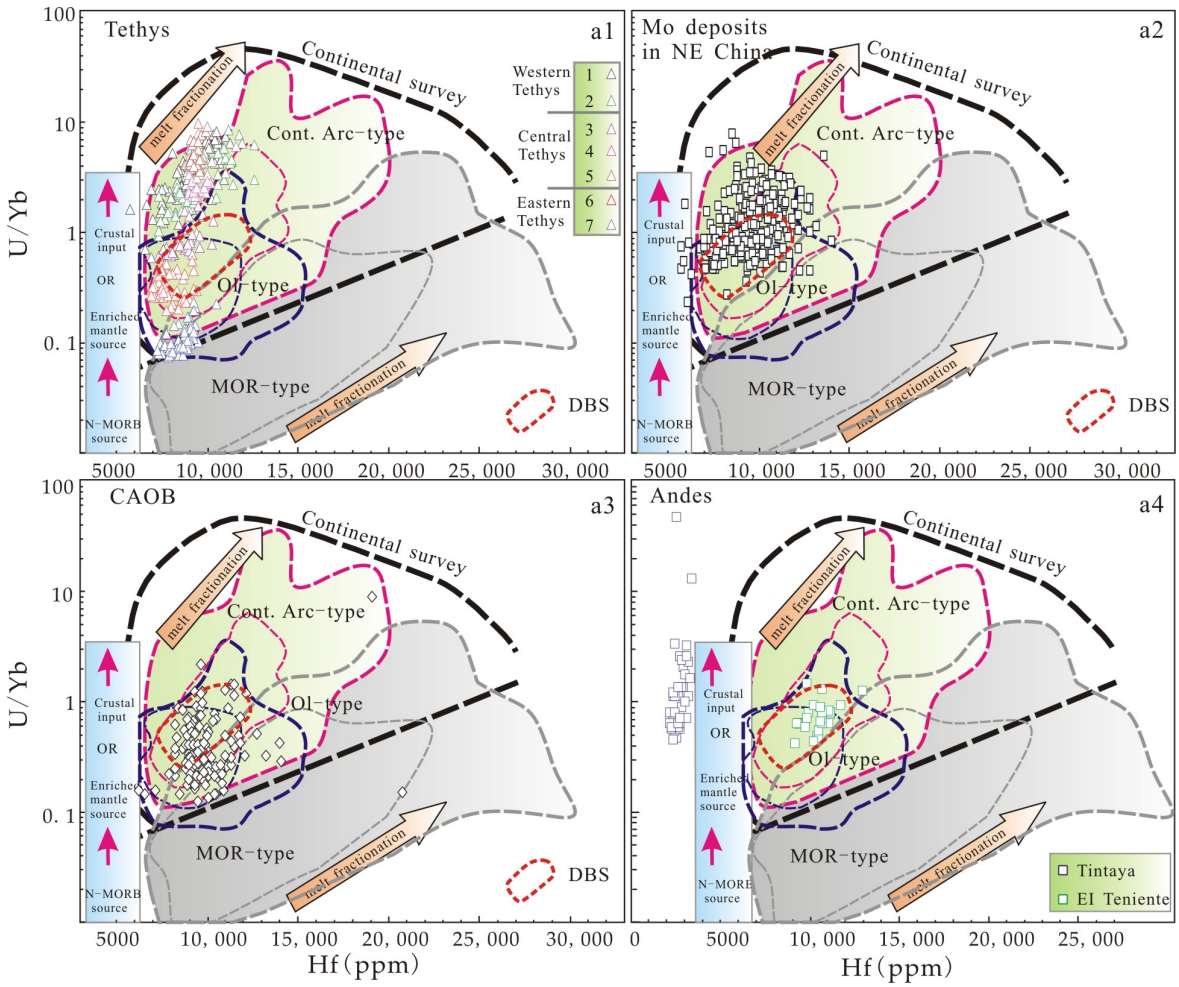
Tethys
a1
Mo deposits
in NE China
a2
CAOB
a3
Andes
a4
Continental survey
melt fractionation
Cont. Arc-type
Ol-type
MOR-type
DBS
Crustal input
OR
Enriched mantle source
N-MORB source
Western Tethys
Central Tethys
Eastern Tethys
1
2
3
4
5
6
7
Tintaya
El Teniente
U/Yb
Hf(ppm)
100
10
1
0.1
5000
10,000
15,000
20,000
25,000
30,000
0

(**a**)

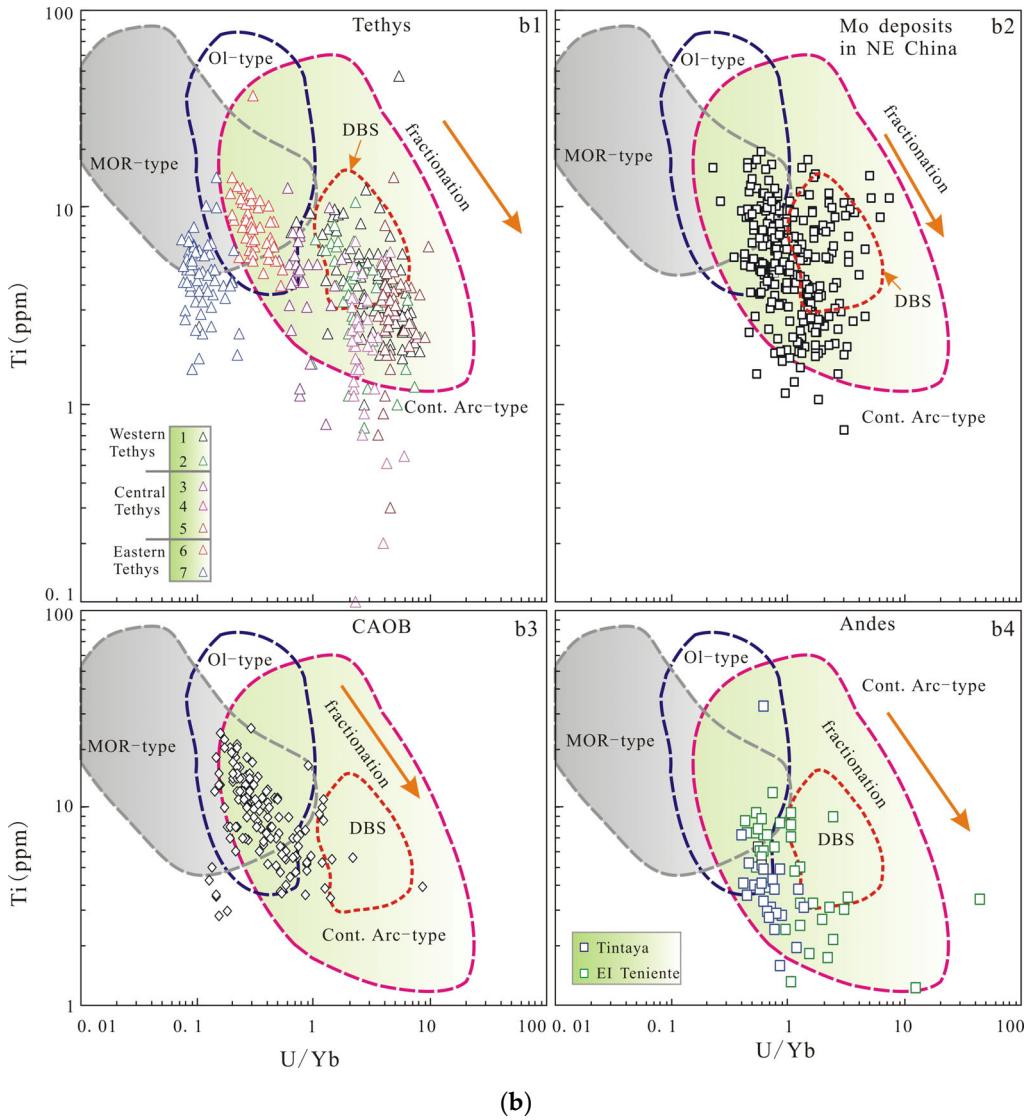


(**b**)

**Figure S5.** Tectono-magmatic setting discrimination diagrams of (**a**) U/Yb versus Hf, and (**b**) Ti versus U/Yb based on trace elements of zircons for porphyry deposits in the world famous metallogenic belts. Note: in Figure S5a,b, (**a1, b1**) Tethys metallogenic belt, (**a2**, **b2**) Mesozoic Mo deposits in NE China, (**a3**, **b3**) metallogenic belt of CAOB, and (**a4**, **b4**) Central Andes metallogenic belt. The fields of Cont. Arc-type, MOR-type and OI-type are the same as Figure 7a,b. In Figure S5a (**a1**), the triangles with numbers refer to names of deposits in Tethys belt, which are the same as in Table S2.

## References


1. Zeng, Q.D.; Liu, J.M.; Chu, S.X.; Wang, Y.B.; Sun, Y.; Duan, X.X.; Zhou, L.L.; Qu, W.J. Re-Os and U-Pb geochronology of the Duobaoshan porphyry Cu-Mo-(Au) deposit, Northeast China, and its geological significance. *J. Asian Earth Sci.* **2014**, *79*, 895–909.
2. Zhao, C.; Qin, K.Z.; Song, G.X.; Li, G.M. Switch of geodynamic setting from the Paleo-Asian ocean to the Mongol-Okhotsk ocean: Evidence from granitoids in the Duobaoshan ore field, Heilongjiang province, Northeast China. *Lithos* **2019**, *336*, 202–220.
3. Shen, P.; Hattori, K.; Pan, H.D.; Jackson, S.; Seitmmuratova, E. Oxidation condition and metal fertility of granitic magmas: Zircon trace-element data from porphyry Cu deposits in the Central Asian Orogenic belt. *Econ. Geol.* **2015**, *110*, 1861–1878.
4. Shu, Q.H.; Chang, Z.S.; Lai, Y.; Hu, X.L.; Wu, H.Y.; Zhang, Y.; Wang, P.; Zhai, D.G.; Zhang, C. Zircon trace elements and magma fertility: Insights from porphyry (-skarn) Mo deposits in NE China. *Mineralium Deposita* **2019**, *54*, 645–656, doi:10.1007/s00126-019-00867-7.
5. Jiang, Y.H.; Jiang, S.Y.; Ling, H.F.; Dai, B.Z. Low-degree melting of a metasomatized lithospheric mantle for the origin of Cenozoic Yulong monzogranite-porphyry, east Tibet: Geochemical and Sr-Nd-Pb-Hf isotopic constraints. *Earth Planet. Sci. Lett.* **2006**, *241*, 617–633.

6. Li, J.X.; Qin, K.Z.; Li, G.M.; Cao, M.J.; Xiao, B.; Chen, L.; Zhao, J.X.; Evans, N.J.; McInnes, B.I.A. Petrogenesis and thermal history of the Yulong porphyry copper deposit, Eastern Tibet: Insights from U-Pb and U-Th/He dating, and zircon Hf isotope and trace element analysis. *Mineral. Petrol.* **2012**, *105*, 201–221.
7. Wang, G.G.; Ni, P.; Yao, J.; Wang, X.L.; Zhao, K.D.; Zhu, R.Z.; Xu, Y.F.; Pan, J.Y.; Li, L.; Zhang, Y.H. The link between subduction-modified lithosphere and the giant Dexing porphyry copper deposit, South China: Constraints from high-Mg adakitic rocks. *Ore Geol. Rev.* **2015**, *67*, 109–126.
8. Chelle-Michou, C.; Chiaradia, M.; Ovtcharova, M.; Ulianov, A.; Wotzlaw, J.F. Zircon petrochronology reveals the temporal link between porphyry systems and the magmatic evolution of their hidden plutonic roots (the Eocene Coroccohuayco deposit, Peru). *Lithos* **2014**, *198*, 129–140.
9. Chelle-Michou, C.; Chiaradia, M.; Béguelin, P.; Ulianov, A. Petrological evolution of the magmatic suite associated with the coroccohuayco Cu (-Au-Fe) porphyry-skarn deposit, Peru. *J. Petrol.* **2015**, *56*, 1829–1862.
10. Cooke, D.R.; Hollings, P.; Walshe, J.L. Giant porphyry deposits: Characteristics, distribution, and tectonic controls. *Econ. Geol.* **2005**, *100*, 801–818.
11. Muñoz, M.; Charrier, R.; Fanning, C.M.; Maksaev, V.; Deckart, K. Zircon trace element and O-Hf isotope analyses of mineralized intrusions from El Teniente ore deposit, Chilean Andes: Constraints on the source and magmatic evolution of porphyry Cu-Mo related magmas. *J. Petrol.* **2012**, *53*, 1091–1122.